

---

# TEST-TIME ADVERSARIAL DEFENSE WITH OPPOSITE ADVERSARIAL PATH AND HIGH ATTACK TIME COST

---

A PREPRINT

**Cheng-Han Yeh & Kuanchun Yu & Chun-Shien Lu**

Institute of Information Science

Academia Sinica

Taipei, Taiwan (ROC)

{jerryyeh,mikeyu1012,lcs}@iis.sinica.edu.tw

May 20, 2025

## ABSTRACT

Deep learning models are known to be vulnerable to adversarial attacks by injecting sophisticated designed perturbations to input data. Training-time defenses still exhibit a significant performance gap between natural accuracy and robust accuracy. In this paper, we investigate a new test-time adversarial defense method via diffusion-based recovery along opposite adversarial paths (OAPs). We present a purifier that can be plugged into a pre-trained model to resist adversarial attacks. Different from prior arts, the key idea is excessive denoising or purification by integrating the opposite adversarial direction with reverse diffusion to push the input image further toward the opposite adversarial direction. For the first time, we also exemplify the pitfall of conducting AutoAttack (Rand) for diffusion-based defense methods. Through the lens of time complexity, we examine the trade-off between the effectiveness of adaptive attack and its computation complexity against our defense. Experimental evaluation along with time cost analysis verifies the effectiveness of the proposed method.

**Keywords** Adversarial Defense · Adversarial Purification · Diffusion Model

## 1 Introduction

### 1.1 Background

It has been well known that deep learning models are vulnerable to adversarial attacks by injecting (imperceptible) adversarial perturbations into the data that will be input to a neural network (NN) model to change its normal predictions Athalye et al. [2018], Carlini et al. [2019], Croce et al. [2023], Frosio and Kautz [2023], Goodfellow et al. [2015], Gowal et al. [2021], Madry et al. [2018], Venkatesh et al. [2023]. Please also see Chen and Liu [2023] for a recent review on the adversarial robustness of deep learning models. It can be found from the literature that adversarial attacks defeat their defense counterparts easily and rapidly, and there is still a gap between natural accuracy and robust accuracy.

The study of adversarial defense in resisting adversarial attacks can be divided into two categories: (1) Adversarial training/Training-time defense Gowal et al. [2021], Hsiung et al. [2023], Huang et al. [2023], Suzuki et al. [2023], Wang et al. [2019, 2023], Wu et al. [2020], Zhang et al. [2019]; and (2) Input pre-processing/Test-time defense Alfarra et al. [2022], Chen et al. [2022], Hill et al. [2020], Ho and Vasconcelos [2022], Nie et al. [2022], Wang et al. [2022], Wu et al. [2022], Yoon et al. [2021]. Adversarial training utilizes adversarial examples derived from the training data to enhance the robustness of the classifier. Despite the effort in training-time defense, we do see (RobustBench Croce et al. [2021]) there is still a remarkable gap between natural accuracy and robust accuracy.

Different from the training-time defense paradigm, in this paper, we propose a new test-time adversarial defensive method by pre-processing data in a way different from the prior works. It is a kind of purifier and serves as a plug-and-play module that can be used to improve the robustness of a defense method once our mod-

ule is incorporated as a pre-processor. Specifically, the formulation of processing the input data is derived as:  $\min_{\phi, \theta} \mathbb{E} [\max_{x' \in B(x)} \mathcal{L}((f_\phi \circ g_\theta)(x'), y)]$ , where  $x'$  denotes the adversarial example corresponding to clean image  $x$  with label  $y$ ,  $B(\cdot)$  is the threat model,  $f_\phi$  is the image classifier parameterized by  $\phi$ , and  $g_\theta$  is a pre-processor.

A key to test-time defense is the design of pre-processor or denoiser (e.g.,  $g_\theta$ ), which aims at denoising an adversarial example to remove the added perturbations. Intuitively, the goal is to have the denoised image as close to the original one so as to achieve perceptual similarity.

## 1.2 Related Works

We introduce representative test-time adversarial defense methods Alfarra et al. [2022], Ho and Vasconcelos [2022], Hill et al. [2020], Yoon et al. [2021], Nie et al. [2022], Wang et al. [2022], Wu et al. [2022] that share the same theme as our method. Please also see Sec. A in the Supplementary for details of Hill et al. [2020], Yoon et al. [2021], Wang et al. [2022], Wu et al. [2022].

In Alfarra et al. [2022], a defense method is proposed by connecting an anti-adversary layer with a pre-trained classifier  $f_\phi$ . Given an input image  $x$ , it will be first sent to the anti-adversary layer for generating anti-adversarial perturbation  $\gamma$  by solving an optimization problem. As the name implies, in most cases, the direction  $\gamma$  will be opposite to the direction of adversarial perturbation. The resultant purified image  $x + \gamma$  is then used for classification.

DISCO Ho and Vasconcelos [2022] is proposed as a purification method to remove adversarial perturbations by localized manifold projections. The author implemented it with an encoder and a local implicit module, which is leveraged by the architecture called LIIF Chen et al. [2021], Chen and Zhang [2019], where the former produces per-pixel features and the latter uses the features in the neighborhood of query pixel for predicting the clean RGB value.

In DiffPure Nie et al. [2022], given an input (clean or adversarially noisy), the goal is to obtain a relatively cleaner version through a series of forward and reverse diffusion processes. Moreover, a theoretical guarantee is derived that, under an amount of Gaussian noise added in the forward step, adversarial perturbation may be removed effectively. This is independent of the types of adversarial perturbations, making DiffPure defend against unseen attacks.

Recently, the robustness of diffusion-based purifiers is considered overestimated. Lee and Kim [2023] provides recommendations for robust evaluation, called *surrogate process*, and shows that defense methods may be defeated under the surrogate process. Kang et al. [2024] proposes DiffAttack, a new attack against diffusion-based adversarial purification defenses, that can overcome the challenges of attacking diffusion models, including vanishing/exploding gradients, high memory costs, and large randomness. The use of a segment-wise algorithm allows attacking with much longer diffusion lengths than previous methods.

Although the aforementioned purification-based adversarial defense methods show promising performance in resisting adversarial attacks, Croce et al. [2022] argues that their evaluations are ineffective in two aspects: (i) Incorrect use of attacks or (ii) Attacks used for evaluation are not strong enough. However, the authors also mentioned test-time defense complicates robustness evaluation because of its complexity and computational cost, which impose even more computations for the attackers.

## 1.3 Motivation

Let us take image classification as an example, where clean/natural accuracy is the classification accuracy for benign images and robust accuracy is measured for adversarial samples. However, we argue that “perceptually similar” does not mean adversarial robustness as it is not guaranteed to entirely remove the adversarial perturbations such that the residual perturbations still have an impact on changing the prediction of a learning model. On the contrary, we propose to purify the input data along the direction of opposite adversarial paths (OAPs) excessively, as shown in Fig. 1.

Conceptually, if we add the adversarial perturbation along the opposite direction of Projected Gradient Descent (PGD) Madry et al. [2017], denoted as “ $-adv$ ,” to a given data, robust accuracy can be improved. To gain an insight that excessive denoising (more than one step along the opposite gradient) is advantageous in resisting attacks, a simple experiment was conducted by moving each data point  $x$  to the new position  $x^K$  through  $K$  iterations of opposite adversarial perturbation, according to the ground truth label and classifier. Given each kind of  $x^K$ , the accuracy change is illustrated in Table 1.

Moreover, motivated by Croce et al. [2022], our defense method also aims to complicate the computation of adaptive adversarial attacks.

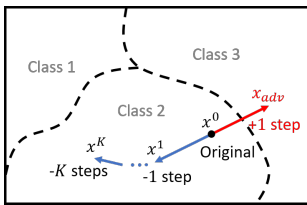


Figure 1: Concept diagram of new reference point generation via  $K$  consecutive purifications along opposite adversarial paths (OAPs).

Table 1: Pre-processing the training dataset by adding  $K$  steps of  $-adv$  (via PGD (Madry et al. [2017]); see Fig. 1) and feeding to a non-defense classifier (ResNet-18 (He et al. [2016])) pre-trained on CIFAR-10 (Krizhevsky et al. [2009]) for testing.  $K = 0$  indicates original data.

## 1.4 Contributions

Different from prior works, the concept of OAP can be incorporated into any training scheme of purifiers, and the OAP-based purifier can also become a part of modules in other defense processes. For instance, OAP-based purifiers can provide additional directions within reverse diffusion, whereas diffusion models alone Song et al. [2020] (baseline model in DiffPure) only provide direction to generate images. Unlike the traditional purification methods, we do not use *classifier-generated labels* (e.g. Anti-Adv Alfarra et al. [2022]) in our baseline purifier during testing. On the contrary, combining the proposed baseline purifier with the reverse diffusion process provides reference directions pointing to a safer area during the purification process.

Contributions of this work are summarized as follows:

(1) We are first to present the idea of excessive denoising along the opposite adversarial path (OAP) as the baseline purifier for adversarial robustness (Sec. 3.1). (2) We integrate the OAP baseline purifier and conditional reverse diffusion as a sophisticated adversarial defense that can be interpreted as moving purified data toward the combination of directions from the score-based diffusion model and baseline purifier (Sec. 3.2). (3) To complicate the entire defense mechanism by complicating the computation overhead of adaptive attacks accordingly, we study a double diffusion path cleaning-based purifier (Sec. 3.3). This creates a trade-off between the attack effectiveness and attack computation. (4) For the first time, we exemplify the pitfall of conducting AutoAttack (Rand) for diffusion-based adversarial defense methods (Sec. 3.4).

## 2 Preliminary

### 2.1 Basic Notation

In the paper,  $x$  denotes an input image,  $\hat{x}$  denotes a recovered image or overly denoised/purified image,  $x_{adv}$  denotes an adversarial image,  $y$  is a ground-truth label of  $x$ ,  $\hat{y}$  is a prediction,  $g_\theta$  is a purifier, and  $f_\phi$  is a pre-trained classifier.

For the diffusion model, the forward process is denoted by  $q(\cdot|\cdot)$  and the backward/reverse process is denoted by  $p_\theta(\cdot|\cdot)$  with parameter  $\theta$ . For  $t \in [0, T]$ ,  $x_t$  represents an image at time step  $t$  during the forward / reverse diffusion process. Usually,  $x_0$  is a clean image and  $x_T \sim \mathcal{N}(0, I)$ .

For the adversarial attack, it modifies the input image  $x$  by adding to it adversarial perturbation  $\delta$  by calculating the gradient of loss according to information leakage of pre-trained NN  $f_\phi$  without changing  $\phi$ , causing  $f_\phi$  to classify incorrectly. According to the leakage level, there are roughly two types of attacks. Please see Sec. B in the Supplementary.

### 2.2 Diffusion Models

Since the diffusion model Sohl-Dickstein et al. [2015], Ho et al. [2020], Song and Ermon [2019], Song et al. [2020] is a baseline model in diffusion-based purifiers, to make this paper self-contained, please refer to Sec. C of Supplementary for a brief introduction to the diffusion model.

### 3 Proposed Method

We describe the proposed test-time adversarial defense method with its flowchart illustrated in Fig. 2.

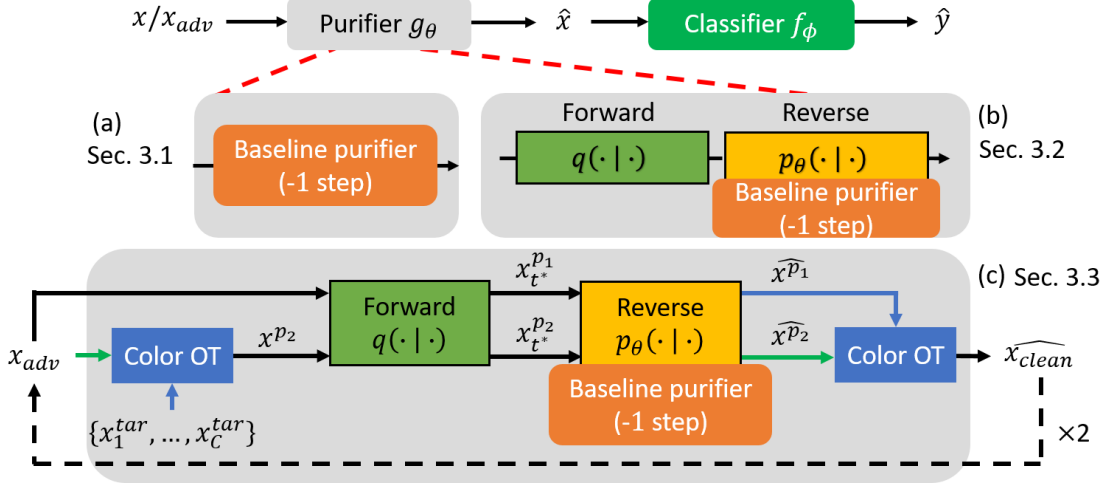


Figure 2: Flowchart of our method. The purifier (gray block) can be one of (a)-(c), where (a) is the proposed baseline purifier, (b) shows the combination of baseline purifier and reverse diffusion, and (c) expands (b) with two diffusion paths. In (c),  $x_1^{tar}, \dots, x_C^{tar}$  are obtained via Eq. (1) from fixed  $C$  images with one image per class. The image in front of Color OT with green/blue arrow is called the source/target image.  $x^{p_2}$  is defined in Eq. (9).

#### 3.1 Baseline Purifier: Opposite Adversarial Path (OAP)

Given a classifier model  $f_\phi$  parameterized by  $\phi$ , a loss function  $\mathcal{L}(x, y, \phi)$ , and a pair of data  $(x, y)$ , the adversarial attack can be computed as:  $x_{adv} = \Pi_{x+\mathcal{S}}(x + \alpha \text{ sign}(\nabla_x \mathcal{L}(x, y, \phi)))$ , where  $\mathcal{S}$  is the set that allows the perceptual similarity between natural and adversarial images. This iterative process aims to find the adversarial image  $x_{adv}$  that maximizes the loss function.

On the other hand, the opposite direction of each iteration points to minimize the loss. Assume now we get an ordinary noisy input  $x_{adv} = x + \delta$  with  $\|\delta\|_p \leq \epsilon_p$  via image processing, a denoiser can push the denoised input close to  $x$  within a non-perceptual distortion. Nevertheless, if the noisy input  $x_{adv}$  is a sophisticated design via adversarial attack, it is too early to claim, depending on the perceptual similarity between  $x$  and  $x_{adv}$ , that the denoised image can be free from being affected by adversarial perturbations. We argue that if we properly push the denoised image further away from the decision boundary, the downstream classifier can still successfully classify the input since the direction we push points to a lower loss area on the input-loss surface, as illustrated in Fig. 1. Also note that the *plug-and-play* module lies under the setting that the baseline purifier is only trained on a given attack (*e.g.*, PGD- $\ell_\infty$ -7), which is independent of the attacks (*e.g.*, PGD- $\ell_\infty$ -40, AutoAttack, and BPDA+EOT) used in testing. In addition, the diffusion model is pre-trained (Sec. 3.2) and does not involve adversarial examples during its training.

##### 3.1.1 New Reference Point Generation

Previous test-time defense methods with a plug-and-play fashion take  $x_{adv}$  as an input and generate the predicted “clean” image  $\hat{x}$ . In our scenario, we want to move a few steps further. Starting from the clean image  $x$ , ground-truth label  $y$ , parameter  $\phi$  and loss function  $\mathcal{L}$  of classifier  $f$ , we can generate a new reference point  $x^K$  for training by:

$$x^k = \Pi_{x^{k-1}+\mathcal{S}}(x^{k-1} - \alpha \text{ sign}(\nabla_{x^{k-1}} \mathcal{L}(x^{k-1}, y, \phi))), \quad (1)$$

for  $1 \leq k \leq K$ , where  $x^0 = x$ . If we iterate Eq. (1), we can get a series of data,  $x^1, x^2, \dots, x^K$ , as illustrated in Fig. 1.

##### 3.1.2 Baseline Purifier Training

In traditional denoising, the goal is to train a purifier that produces a denoised output  $\hat{x}$  from the adversarial input  $x_{adv}$ , denoted as  $x_{adv} \mapsto \hat{x}$ , such that  $\hat{x}$  and  $x$  can be as similar as possible in terms of, say,  $\ell_p$ -norm. We, instead, train the purifier to produce  $\hat{x}^K$  from  $x_{adv}$  that further points toward the opposite adversarial attack direction. We call

-K steps	Non-adapt PGD- $\ell_\infty$ / ResNet-18		Non-adapt AA / WRN-28-10		BPDA / VGG16	
	Clean Acc (%)	Robust Acc (%)	Clean Acc (%)	Robust Acc (%)	Clean Acc (%)	Robust Acc (%)
0	89.57	73.13	89.00	85.00	88.38	47.37
-1	90.71	86.10	91.66	88.79	89.26	56.34
-3	89.53	82.02	90.23	86.14	87.78	59.94
-7	89.33	56.21	89.58	69.04	88.42	52.31

Table 2: Evaluation of DISCO trained with the relation between new reference point and adversarial perturbations by PGD attack generated in ResNet-18. Entire CIFAR-10 testing dataset was used. (Left) Attack: Non-adaptive PGD- $\ell_\infty$ . Test model: ResNet-18. (Middle) Attack: Non-adaptive AutoAttack (AA). Test model: WRN-28-10 Zagoruyko and Komodakis [2017]. (Right) Attack: BPDA. Test model: VGG16 Simonyan and Zisserman [2015].

the resultant  $\widehat{x^K}$  an excessively-denoised image and the model  $g_\theta$  that moves data along the opposite adversarial path (OAP) the ‘‘baseline purifier.’’

In practice, we train a baseline purifier using data pairs  $\{(x_{adv}, x^K)\}$  with a certain number of opposite steps  $K \in \mathbb{N}$ , where  $x^K$  is generated by Eq. (1). The training procedure of  $g_\theta$  is to minimize:

$$\theta^* = \operatorname{argmin}_\theta \|g_\theta(x_{adv}) - x^K\|_1, \quad (2)$$

where  $g_\theta$  can be any existing defense methods (e.g., DISCO Ho and Vasconcelos [2022]). The results of training on different opposite steps are shown in Table 2 with respect to PGD- $\ell_\infty$  Madry et al. [2017], AutoAttack (AA) Croce and Hein [2020], and BPDA Athalye et al. [2018]. We can observe that the idea of the new reference point indeed improves DISCO. Specifically, when  $K = 1$ , the robust accuracy can be improved greatly, but it decreases as  $K$  goes larger. The results are somewhat inconsistent with those in Table 1. The reason we conjecture is that the experiment presented in Table 1 was conducted using the ground-truth label to move data step-by-step, but it is not in Table 2. Besides, as  $K$  increases, the distance that needs to push the data increases as well, similar to the effect of large step size in gradient descent, e.g., coarse gradient estimation near the decision boundary. Therefore, based on the empirical observations, we will empirically set  $K = 1$  for learning the opposite direction of an adversarial attack during training.

On the other hand, we will later demonstrate that OAP is a powerful module readily to be incorporated with existing adversarial defenses (e.g., DISCO) in improving both the clean and robust accuracy.

### 3.2 Diffusion-based Purifier with OAP Prior

In Sec. 3.1, we have witnessed the merit of baseline purifier based on OAP in improving robustness against adversarial attacks. This data moving trick also motivates us to study how to incorporate OAP prior and diffusion models as a stronger adversarial defense.

We first propose to integrate the idea of opposite adversarial paths with the reverse diffusion process (e.g., guided diffusion Dhariwal and Nichol [2021], ILVR Choi et al. [2021], and DDA Gao et al. [2023]) to achieve a similar goal of pushing the input image further toward the opposite adversarial direction. More importantly, for each step in the reverse diffusion process, the purifier is used to provide a direction that points to  $x^K$ .

To this end, according to Eq. (13) of guided diffusion described in Sec. C in Supplementary, by taking logarithm and gradient with respect to  $x_{t-1}$  Dhariwal and Nichol [2021], we can derive

$$\begin{aligned} & \nabla_{x_{t-1}} \log p_\theta(x_{t-1}|x_t, y) \\ &= \nabla_{x_{t-1}} \log p_\varphi(x_{t-1}|x_t) + \nabla_{x_{t-1}} \log p_\phi(y|x_{t-1}), \end{aligned} \quad (3)$$

where  $t$  denotes the diffusion time step. Based on Langevin dynamics, we get a sampling chain on  $x_{t-1}$  as:

$$x_{t-1} \leftarrow x_t + \nabla_{x_{t-1}} \log p_\varphi(x_{t-1}|x_t), \quad (4)$$

where we get the first direction (specified by  $p_\varphi$ ) of moving to  $x_{t-1}$ . However, if we want to generate  $x_{t-1}$  by moving along the direction given  $x_t$  and  $y$ , we have to introduce the second direction (specified by  $p_\phi$ ) to move to  $x_{t-1}$  given condition  $y$  based on Eq. (3). Hence, we add  $\nabla_{x_{t-1}} \log p_\phi(y|x_{t-1})$  in the sampling chain (4) as:

$$\begin{aligned} x_{t-1} \leftarrow x_t &+ \nabla_{x_{t-1}} \log p_\varphi(x_{t-1}|x_t) \\ &+ \nabla_{x_{t-1}} \log p_\phi(y|x_{t-1}), \end{aligned} \quad (5)$$

where the last two terms are the same as the RHS of Eq. (3). Note that the second term can be approximated by a model  $\epsilon_\varphi(\cdot)$  that predicts the noise added to the input. According to (11) in Dhariwal and Nichol [2021], it can be used to

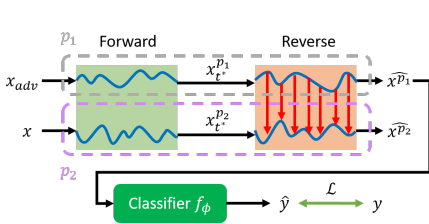


Figure 3: (Ideal model) Red arrows depict directions to minimize  $\ell_2$  distance between the intermediate images of two reverse paths,  $p_1$  and  $p_2$ .  $\mathcal{L}$ : loss function.

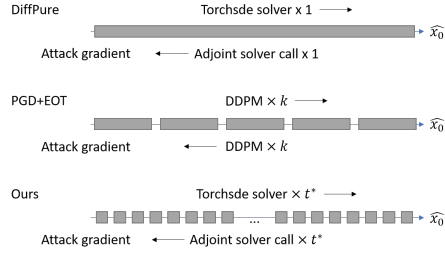


Figure 4: Reverse diffusion process implementations: The original implementation of DiffPure involves only one function call in reverse and adjoint solver calls. The PGD+EOT attack utilizes a surrogate diffusion process with fewer steps than purification steps. However, in our implementation, we use the same number of steps for purification and attack.

derive a score function as:

$$\nabla_{x_{t-1}} \log p_\varphi(x_{t-1}|x_t) = -\frac{\epsilon_\varphi(x_{t-1})}{\sqrt{1-\bar{\alpha}_t}}, \quad (6)$$

where  $\bar{\alpha}_t = \prod_{s=1}^t (1 - \beta_s)$ .

Different from previous works, if  $y$  in the third term of Eq. (5) is replaced with the new reference point  $x^K$ , as described in Eq. (1) of Sec. 3.1, then the term becomes  $\nabla_{x_{t-1}} \log p_\phi(x^K|x_{t-1})$  and represents how to move along the direction to  $x^K$  given  $x_{t-1}$ . This can be set by

$$\begin{aligned} \widehat{x^K} &\leftarrow g_\theta(x_{t-1}); \\ \nabla_{x_{t-1}} \log p_\phi(x^K|x_{t-1}) &\approx \eta(\widehat{x^K} - x_{t-1}), \end{aligned} \quad (7)$$

where  $\eta$  is the step size and  $g_\theta(\cdot)$  is the purifier (see Sec. 3.1) that can approximate the mapping of  $x_{adv} \rightarrow x^K$ . Hence, the purification process can be interpreted as moving toward the combination of directions from the score-based diffusion model Nie et al. [2022], Song and Ermon [2019], Song et al. [2020] and baseline purifier  $g_\theta(\cdot)$ .

### 3.2.1 Connecting the OAP Prior with Diffusion

We are aware that the base purifier has to operate in the domain the same as that in the diffusion reverse process, *i.e.*, they deal with different inputs with noises at different scales. However, according to Eq. (2), the baseline purifier only takes inputs that are adversarially perturbed. Hence, during the training of baseline purifier, we randomly add different scales of noise to the input data so that the base purifier can accommodate the different noise scales in the reverse diffusion process, denoted as:

$$\theta_n^* = \operatorname{argmin}_\theta \mathbb{E}_{p_{data}(x_{adv})} \mathbb{E}_{p_{\sigma_t}(\tilde{x}|x_{adv})} \|g_\theta(\tilde{x}) - x^K\|_1, \quad (8)$$

where  $t$  is uniformly chosen from  $0 \dots t^*$ ,  $\sigma_t$  is the corresponding noise scale at diffusion time step  $t$ , and  $\tilde{x}$  is the perturbed data according to the diffusion process. We replace the baseline purifier  $g_\theta$  in Eq. (7) in Sec. 3.2 with this purifier  $g_{\theta_n}$ .

### 3.3 Diffusion Path Cleaning-based Purifier

In this section, we describe how to further utilize other gradients from different constraints to modify/move our samples toward specific directions. Moreover, the goal is to complicate the entire framework of purifier+classifier so as to complicate the computation of adaptive attacks accordingly while maintaining comparable clean and robust accuracy. We first conduct a test to verify whether such a framework could be affected by such an attack.

In this test, we verify the framework composed of two diffusion paths, denoted as  $p_1$  and  $p_2$ , and a pre-trained classifier  $f_\phi$  (*e.g.*, pre-trained WRN-28-10), as shown in Fig. 3. The adaptive adversarial image  $x_{adv}$  is generated via BPDA+EOT Athalye et al. [2018] as an input to path  $p_1$  while the clean image  $x$  is assumed to be available (ideal case) in path  $p_2$ . In this case, we minimize the  $\ell_2$  distance between the intermediate image in the reverse process  $p_1$  and that in  $p_2$ , which gives a direction to make  $p_1$  close to  $p_2$ . Finally, the output  $\widehat{x^{p1}}$  is feed into the classifier  $f_\phi$  for prediction. We obtain

the natural acc of 93.5% and robust acc of 93.0% from CIFAR-10. This provides us a hint that the diffusion path  $p_1$  should be maintained relatively clean (e.g., both the input and reverse diffusion process in path  $p_1$  are as clean as those in path  $p_2$ ) so that the output of  $p_1$ , which is the recovered image  $\widehat{x}^{p_1}$ , is purified enough.

Therefore, the motivation here is to expand the idea of the opposite adversarial direction in modifying (i) the input for arriving at a safer area and (ii) the entire path for purification. Nevertheless, the clean image  $x$  corresponding to  $x_{adv}$  required for the second path  $p_2$  is absent during testing. In addition, it is known that adversarial perturbation is added to an image and causes imperceptible changes. In view of this, we resort to generating purified images as input to  $p_2$  using the new reference point strategy, as described in Eq. (1) of Sec. 3.1.

Conceptually, the idea of generating the input to path  $p_2$  that guides path  $p_1$  is to transfer pixel values from the source image (adversarial image) to the other target image (clean/purified image), which can be treated as finding the optimal transport plan that moves every 3D point (RGB value) in a source point cloud to a target point cloud with the minimum cost (e.g., in terms of  $\ell_2$  distance between two point clouds). Fortunately, we can use non-attack images, which are the training data, combined with Eq. (1) to produce excessively denoised target images for diluting the attack perturbation.

Based on the above test and observations, we now describe the proposed method for cleaning the diffusion path with adversarial images as input. The flowchart is illustrated in Fig. 2(c). First, suppose we have  $x_{adv}$  as the source image, it will be processed by color transfer with optimal transport Feydy et al. [2019], which is denoted as “Color OT” in Fig. 2(c), using the images coming from the training dataset. To this end, we pick  $C$  images with one image per class, where  $C$  stands for the number of classes. By using Eq. (1) to generate new reference points from these picked images, we have the target images  $x_1^{tar}, \dots, x_C^{tar}$  for “Color OT” to change/purify the adversarial pixels in  $x_{adv}$ . The  $C$  target images will not be picked again throughout the testing so that there is no randomness.

Second, after finding the  $x_j^{tar}$  that has the lowest Sinkhorn divergences  $S_\varepsilon$  (Eq. (3) in Feydy et al. [2019]) with  $x_{adv}$ , we then use color transfer  $f_{CT}$  to modify  $x_{adv}$  with reference to  $x_j^{tar}$ . The output is denoted as  $x^{p_2}$ . The purification procedure is specified as:

$$j = \underset{i \in \{1, \dots, C\}}{\operatorname{argmin}} S_\varepsilon(x_{adv}, x_i^{tar}); \quad x^{p_2} = f_{CT}(x_{adv}, x_j^{tar}). \quad (9)$$

As our starting point,  $x^{p_2}$  goes into the diffusion process, as shown in Fig. 2(c). This ensures all pixel values in  $x^{p_2}$  are not from  $x_{adv}$ . To make it clear, examples of the intermediate images generated from the diffusion process in Fig. 2(c) are illustrated in Fig. 5 of Sec. D in the Supplementary.

Third, we put  $x_{adv}$  and  $x^{p_2}$  into the diffusion model and set  $t^*$ , which is the optimal time step Nie et al. [2022] to remove the adversarial noise. We maintain two paths: the path with superscript  $p_1$  for denoising the color values and the path with superscript  $p_2$  for recovering the image. Unlike the test in Fig. 3, during the reverse diffusion process, we do not use  $p_2$  to pull  $p_1$ , since  $x^{p_2}$  is generated by  $f_{CT}$ . Instead, we use “baseline purifier+reverse diffusion” described in Sec. 3.2 on one path,  $p_1$ . Therefore, after the reverse diffusion process, the image  $\widehat{x}^{p_2}$  will refer to the denoised image  $\widehat{x}^{p_1}$  as the target for  $f_{CT}$  to restore the colors, which is denoted as  $\widehat{x}^{clean}$ . This is because  $\widehat{x}^{p_2}$  is still a color-transferred image after the diffusion model, but the output from  $p_2$  in the aforementioned test (Fig. 3) starts from the ideal clean image  $x$  without needing color restoration. The whole process will be iterated again with starting point  $\widehat{x}^{clean}$  and  $t^*$  being halved at each iteration. Please see Algorithm 1 in Sec. E of Supplementary in describing the entire procedure.

### 3.4 Granularity of Gradient Approximation in Realizing Powerful Adaptive AutoAttack

We present to implement a more powerful adaptive AutoAttack via granularity of gradient approximation in order not to overestimate robustness. Actually, our implementation requires the output in each step from `torchsde` in the diffusion reverse process, which starts from  $x_{t^*}$  and calls `torchsde` to produce the output  $x_{t^*-1}$  of next time step till we get the final image  $\hat{x}$ . Hence, if one understands the mechanism of using *adjoint method* as BPDA correctly, gradient computation in the reverse diffusion process will demand the same amount of calls of *adjoint method* as in that of `torchsde`. We have to particularly point out that this is different from DiffPure Nie et al. [2022], where the authors only used one `torchsde` call for the final image and one call of *adjoint method* for computing the gradient. We believe the granularity (one call vs. multiple calls of *adjoint method*) of gradient approximation causes the performance difference, and the use of multiple calls indeed provides AutoAttack with sufficient information to generate a more powerful adversarial perturbation.

To verify our finding, we have observations across different datasets in Table 3. First, we selected a subset from CIFAR-10 testing dataset consisting of 64 images, then generated the corresponding adversarial examples from adaptive AutoAttack (Rand) with 20 EOT via two different implementations, including (1) AutoAttack (Rand-DiffPure): Original code from DiffPure Nie et al. [2022] using one `torchsde` function call and (2) AutoAttack (Rand-Ours): Our own implementation that pulls the output  $x_t$  at each time step from `torchsde` solver, which means 100 `torchsde` function calls. See Fig. 4 for comparison of different implementations of reverse diffusion process.

We can see from Table 3 that in comparison with AutoAttack (Rand-DiffPure), the defense capability of DiffPure is remarkably reduced (the accuracy in boldface) when the adversarial examples generated from AutoAttack (Rand-Ours) are present, obviously indicating robustness overestimation. Actually, it is evidence of revealing that our implementation can let attackers create stronger adversarial examples and can be used as a proxy to attack diffusion-based purifiers. Also, this finding sheds light on whether using *adjoint method* hides the information used for creating stronger adversarial examples in an adaptive AutoAttack setting.

Finally, since DiffPure Nie et al. [2022] has not been evaluated in Croce et al. [2022], it is believed that this simple trick of implementation that creates stronger AutoAttack (Rand) can be an easy way of attacking test-time adversarial defense purifiers and a promising supplement to Croce et al. [2022]. In the following experimental evaluations, this kind of adjoint strategy will be used in implementing stronger adaptive attacks.

AutoAttack	(Rand-DiffPure)	(Rand-Ours)	AutoAttack	(Rand-DiffPure)	(Rand-Ours)	AutoAttack	(Rand-DiffPure)	(Rand-Ours)
DiffPure	76.56%	<b>64.06%</b>	DiffPure	26.56%	<b>20.31%</b>	DiffPure	46.88%	<b>28.13%</b>

Table 3: Robust accuracy for adversarial examples (Adv) generated from different implementations of diffusion purification under adaptive AutoAttack (Rand) with 20 EOT. Our implementation uses output in every time step from `torchsde`, whereas DiffPure Nie et al. [2022] uses `torchsde` without accessing the intermediate outputs, which is encapsulated in `torchsde` function call. Left: CIFAR-10/WRN-28-10; Middle: CIFAR-100/WRN-28-10; Right: ImageNet/ResNet-18.

Defense Methods	Clean Accuracy (%)	Robust Accuracy (%)	Attacks
No defense	94.78	0	PGD- $\ell_\infty$
AWP Wu et al. [2020]*	88.25	60.05	AutoAttack (Standard)
Anti-Adv Alfarra et al. [2022]* + AWP Wu et al. [2020]	88.25	79.21	AutoAttack (Standard)
DISCO Ho and Vasconcelos [2022]*	89.26	82.99	PGD- $\ell_\infty$
DISCO Ho and Vasconcelos [2022] + <b>our OAP</b> ( $K = 1$ )	<b>92.5±2.06</b>	88.29±3.3	PGD- $\ell_\infty$
DiffPure Nie et al. [2022]	88.06±2.65	87.21±2.28	PGD- $\ell_\infty$
DiffPure Nie et al. [2022]	88.15±2.86	87.71±2.12	AutoAttack (Standard)
SOAP Shi et al. [2021]*	96.93	63.10	PGD- $\ell_\infty$
Hill et al. Hill et al. [2020]*	84.12	78.91	PGD- $\ell_\infty$
ADP ( $\sigma = 0.1$ ) Yoon et al. [2021]*	93.09	85.45	PGD- $\ell_\infty$
Ours (Sec. 3.2)	90.77±2.25	<b>88.48±2.04</b>	PGD- $\ell_\infty$
Ours (Sec. 3.2)	<b>90.46±2.36</b>	<b>89.06±2.62</b>	AutoAttack (Standard)

Table 4: Non-adaptive robustness comparison between our method and state-of-the-art methods. Classifier: WRN-28-10. Asterisk (\*) indicates that the results were excerpted from the papers. Boldface indicates the best performance for each attack. Note that, by incorporating our *Opposite Adversarial Path* (OAP) prior, the clean and robust accuracy of DISCO can be greatly increased.

Defense Methods	Clean Accuracy (%)	Robust Accuracy (%)	Attack time cost (sec.)	Attacks
No defense	94.78	0	N/A	BPDA+EOT
DiffPure	<b>92.38±1.86</b>	80.92±3.53	592.92	BPDA+EOT
Hill et al.*	84.12	54.90	N/A	BPDA+EOT
ADP ( $\sigma = 0.1$ )*	86.14	70.01	N/A	BPDA+EOT
Ours (Sec. 3.3)	92.08±1.99	<b>81.25±3.62</b>	<b>6880.97</b>	BPDA+EOT
DiffPure	96.88	46.88	3632.94	PGD+EOT
Ours (Sec. 3.3)	<b>100</b>	<b>53.12</b>	<b>22721.90</b>	PGD+EOT
DiffPure	89.02	46.88	N/A	DiffAttack
Ours (Sec. 3.3)	<b>95.31</b>	<b>93.75</b>	<b>20397.27</b>	DiffAttack

Table 5: Adaptive robustness comparison between our method and state-of-the-art methods with attack time cost per image. Classifier: WRN-28-10. Asterisk (\*) indicates that the results were excerpted from the papers. Boldface indicates the best performance for each attack. The attacks include BPDA+EOT, PGD+EOT Lee and Kim [2023], and DiffAttack Kang et al. [2024].

### 3.5 Attack Cost and Time Complexity

We study how to resist adaptive attacks by analyzing and increasing the time cost of breaking the proposed defense models. The results are shown in Table 5. Due to space constraints, please see the time complexity analysis in Sec. F in the Supplementary for details.

## 4 Experiments

We examine the performance of proposed test-time adversarial defense methods, described in Sec. 3.2 and Sec. 3.3.

### 4.1 Datasets and Experimental Settings

Three datasets, CIFAR-10 Krizhevsky et al. [2009], CIFAR-100 Krizhevsky et al. [2009], and ImageNet Deng et al. [2009], were adopted, where the results for CIFAR-100 and ImageNet are shown in Table 3 and Sec. G of Supplementary. All experiments were conducted on a server with Intel Xeon(R) Platinum 8280 CPU and NVIDIA V100.

For a fair comparison, we followed RobustBench Croce et al. [2021] and existing literature to conduct experiments on two popular NN models, including ResNet-18 He et al. [2016] and WRN-28-10 Zagoruyko and Komodakis [2017]. The step size,  $\eta$ , in Eq. (7) of Sec. 3.2 was set as  $2.5 \times 10^{-3}$  and we followed Nie et al. [2022] to set  $t^*$  used in Sec. 3.2 and Sec. 3.3 as 0.1. Since  $t^* = 0.1$ , the number of steps required in the reverse process is 100, where the step size  $dt$  for `torchsde` solver is set to 1e-3. We set  $\varepsilon = 0.05$  in Eq. (9), which is the default setting in the official package (GeomLoss) Feydy et al. [2019]. For all attacks, we used  $\ell_\infty$  and set perturbation  $\|\delta\|_\infty \leq 8/255$ .

For training, the only model that needs to be trained is the baseline purifier  $g_{\theta_n}$  with  $K = 1$ , which we chose DISCO Ho and Vasconcelos [2022] as the baseline to be combined with our new reference point generation in Eq. (1) with  $K = 1$  throughout the experiments. In computing the attack gradient per step ( $K$ ), we used PGD- $\ell_\infty$  with 7 iterations. For testing the diffusion-based purifiers, we followed the testing paradigm described in DiffPure Nie et al. [2022], including the uses of 24 random subsets (each contains 64 images) for AutoAttack and 15 random subsets (each contains 200 images) for BPDA+EOT from CIFAR-10 testing dataset.

### 4.2 Adversarial Robustness Evaluations

Several types of adversarial attacks, including (A1) non-adaptive attacks (PGD- $\ell_\infty$  Madry et al. [2017], AutoAttack (Standard) Croce and Hein [2020]), (A2) adaptive attacks (BPDA+EOT Athalye et al. [2018], PGD+EOT Lee and Kim [2023] and DiffAttack Kang et al. [2024]), and (A3)  $\ell_2$ -norm optimization-based attacks and black-box attacks, including C&W attack Carlini and Wagner [2016], SPSA Uesato et al. [2018], and the targeted black-box attack in both settings (nonadaptive/adaptive), were adopted. Please see Sec. G of Supplementary for the evaluation of (A3).

For AutoAttack, we utilized the package AutoAttack Croce and Hein [2020] with  $\ell_\infty$ , in which it has two settings: (1) “Standard,” which includes APGD-CE, APGD-DLR, FAB, and Square Attack and (2) “Rand,” which includes APGD-CE and APGD-DLR with Expectation Over Time (EOT) Athalye et al. [2018] in case of models with stochastic components. To the most extreme case in which the attacker knows every detail about our framework of “purifier+classifier,” we utilized BPDA (*adjoint method* Li et al. [2020]) to bypass purifiers and EOT to combat the randomness in purifiers. As mentioned in Sec. 3.4, our adjoint strategy will be used to implement stronger adaptive attacks in order to avoid robustness overestimation.

Robustness performance was measured by clean/natural accuracy (Clean Acc) for benign samples and robust accuracy (Robust Acc) for adversarial samples. Several test-time adversarial defense methods, including Anti-Adv Alfarra et al. [2022], DISCO Ho and Vasconcelos [2022], DiffPure Nie et al. [2022], SOAP Shi et al. [2021], Hill et al. Hill et al. [2020], and ADP Yoon et al. [2021], were adopted for comparison. Tables 4 and 5 show the robustness evaluations and indicate that our methods either outperform or are comparable with prior works.

The experiment in Table 4 is under the setting of non-adaptive attacks (PGD- $\ell_\infty$  with 40 iterations and AutoAttack (Standard)), in which the attacker only knows the information of the downstream classifier. According to Alfarra et al. [2022], we specifically point out that the authors used the robustly trained classifier, Adversarial Weight Perturbation (AWP) Wu et al. [2020], as the testing classifier. So, except Alfarra et al. [2022], we used a normally trained classifier throughout the experiments.

Table 5 shows the results obtained under adaptive attacks, including stronger ones like PGD+EOT Lee and Kim [2023] and DiffAttack Kang et al. [2024]. For the two kinds of AutoAttack (Rand) described in Sec. 3.4, please refer to Table 3. Since most diffusion-based purifiers exhibit randomness, we utilized the “EOT” setting for randomness, and “BPDA” for bypassing the reverse process of diffusion-based methods, which use the *adjoint method* to calculate the gradient of such process. We also provide the time needed to attack an image (attack time cost) against a defense method. Besides, according to the dual-paths design of Sec. 3.3, all adaptive attacks have to attack both paths. As a result, our defense experiences TWICE stronger attacks than other single-path methods since gradients are obtained from two paths. In other words, attacks are computed twice.

More specific, we can see from Table 5 that, in addition to accuracy, the time costs the attackers need to generate attack examples for our defense method are greatly higher than those for other defense methods. If the attackers would like to shorten computations of generating adversarial examples, the number of iterations of conducting attacks or the number of EOT need to be reduced, thereby weakening the attack performance. Take BPDA+EOT as an example: the total time to finish a batch testing on DiffPure costs less than 1 day but it costs 2 days to test on our proposed method under the same setting with 8 V100 GPUs. Moreover, the number of paths in our method (Sec. 3.3) can be flexibly increased to be larger than two to greatly increase the time cost for attackers to generate adaptive attack examples. An accompanying merit is that the robust accuracy of our method in resisting DiffAttack is rather high because DiffAttack focuses on attacking the only one path by computing the gradient on it without meeting our dual path strategy.

## 5 Conclusions & Limitations

We have presented a new test-time adversarial defense method by excessively denoising the incoming input image along the opposite adversarial path (OAP). This OAP prior can be readily plugged into the existing defense mechanisms for robustness improvement. Meanwhile, we exemplify, for the first time, the pitfall of conducting AutoAttack (Rand) for diffusion-based adversarial defense methods. However, we are aware there are several attacks targeting diffusion-based adversarial defenses, and the performance of our proposed method may be overestimated since the gradient computation is approximated.

## References

A. Athalye, N. Carlini, and D. Wagner. Obfuscated gradients give a false sense of security: Circumventing defenses to adversarial examples. In *International Conference on Machine Learning*. PMLR, 2018.

N. Carlini, A. Athalye, N. Papernot, W. Brendel, J. Rauber, D. Tsipras, I. Goodfellow, and A. Madry. On evaluating adversarial robustness. *arXiv preprint arXiv:1902.06705*, 2019.

Francesco Croce, Sylvestre-Alvise Rebuffi, Evan Shelhamer, and Sven Gowal. Seasoning model soups for robustness to adversarial and natural distribution shifts. In *Proceedings of the IEEE/CVF Conference on Computer Vision and Pattern Recognition*, 2023.

Iuri Frosio and Jan Kautz. The best defense is a good offense: Adversarial augmentation against adversarial attacks. In *Proceedings of the IEEE/CVF conference on computer vision and pattern recognition*, 2023.

I. J. Goodfellow, J. Shlens, and C. Szegedy. Explaining and harnessing adversarial examples. In *International Conference on Learning Representations*, 2015.

Sven Gowal, Sylvestre-Alvise Rebuffi, Olivia Wiles, Florian Stimberg, Dan Andrei Calian, and Timothy A Mann. Improving robustness using generated data. *Advances in Neural Information Processing Systems*, 34:4218–4233, 2021.

A. Madry, A. Makelov, L. Schmidt, D. Tsipras, and A. Vladu. Towards deep learning models resistant to adversarial attacks. In *International Conference on Learning Representations*, 2018.

Rahul Venkatesh, Eric Wong, and Zico Kolter. Adversarial robustness in discontinuous spaces via alternating sampling & descent. In *Proceedings of the IEEE/CVF Winter Conference on Applications of Computer Vision*, 2023.

P.-Y. Chen and S. Liu. Holistic adversarial robustness of deep learning models. In *Proceedings of the AAAI Conference on Artificial Intelligence*, 2023.

Lei Hsiung, Yun-Yun Tsai, Pin-Yu Chen, and Tsung-Yi Ho. Towards compositional adversarial robustness: Generalizing adversarial training to composite semantic perturbations. In *Proceedings of the IEEE/CVF Conference on Computer Vision and Pattern Recognition*, 2023.

Bo Huang, Mingyang Chen, Yi Wang, Junda Lu, Minhao Cheng, and Wei Wang. Boosting accuracy and robustness of student models via adaptive adversarial distillation. In *Proceedings of the IEEE/CVF Conference on Computer Vision and Pattern Recognition*, 2023.

Satoshi Suzuki, Shin'ya Yamaguchi, Shoichiro Takeda, Sekitoshi Kanai, Naoki Makishima, Atsushi Ando, and Ryo Masumura. Adversarial finetuning with latent representation constraint to mitigate accuracy-robustness tradeoff. In *ICCV*, 2023.

Yisen Wang, Difan Zou, Jinfeng Yi, James Bailey, Xingjun Ma, and Quanquan Gu. Improving adversarial robustness requires revisiting misclassified examples. In *International conference on learning representations*, 2019.

Zekai Wang, Tianyu Pang, Chao Du, Min Lin, Weiwei Liu, and Shuicheng Yan. Better diffusion models further improve adversarial training. In *International Conference on Machine Learning*, pages 36246–36263. PMLR, 2023.

Dongxian Wu, Shu-Tao Xia, and Yisen Wang. Adversarial weight perturbation helps robust generalization. *Advances in Neural Information Processing Systems*, 33:2958–2969, 2020.

Hongyang Zhang, Yaodong Yu, Jiantao Jiao, Eric Xing, Laurent El Ghaoui, and Michael Jordan. Theoretically principled trade-off between robustness and accuracy. In *International conference on machine learning*, pages 7472–7482. PMLR, 2019.

Motasem Alfarras, Juan C Pérez, Ali Thabet, Adel Bibi, Philip HS Torr, and Bernard Ghanem. Combating adversaries with anti-adversaries. In *Proceedings of the AAAI Conference on Artificial Intelligence*, volume 36, pages 5992–6000, 2022.

J. Chen, X. Wu, Y. Guo, Y. Liang, and S. Jha. Towards evaluating the robustness of neural networks learned by transduction. In *International Conference on Learning Representations*, 2022.

Mitch Hill, Jonathan Craig Mitchell, and Song-Chun Zhu. Stochastic security: Adversarial defense using long-run dynamics of energy-based models. In *International Conference on Learning Representations*, 2020.

Chih-Hui Ho and Nuno Vasconcelos. Disco: Adversarial defense with local implicit functions. *Advances in Neural Information Processing Systems*, 35:23818–23837, 2022.

Weili Nie, Brandon Guo, Yujia Huang, Chaowei Xiao, Arash Vahdat, and Anima Anandkumar. Diffusion models for adversarial purification. In *International Conference on Machine Learning*, 2022.

Jinyi Wang, Zhaoyang Lyu, Dahua Lin, Bo Dai, and Hongfei Fu. Guided diffusion model for adversarial purification. *arXiv preprint arXiv:2205.14969*, 2022. URL <https://arxiv.org/abs/2205.14969>.

Quanlin Wu, Hang Ye, and Yuntian Gu. Guided diffusion model for adversarial purification from random noise. *arXiv preprint arXiv:2206.10875*, 2022. URL <https://arxiv.org/abs/2206.10875>.

Jongmin Yoon, Sung Ju Hwang, and Juho Lee. Adversarial purification with score-based generative models. In *International Conference on Machine Learning*, pages 12062–12072. PMLR, 2021.

F. Croce, M. Andriushchenko, V. Sehwag, E. Debenedetti, N. Flammarion, M. Chiang, P. Mittal, and M. Hein. Robustbench: a standardized adversarial robustness benchmark. *Advances in neural information processing systems, Process. Syst. Datasets and Benchmarks Track*, 2021.

Yinbo Chen, Sifei Liu, and Xiaolong Wang. Learning continuous image representation with local implicit image function. In *Proceedings of the IEEE/CVF conference on computer vision and pattern recognition*, pages 8628–8638, 2021.

Zhiqin Chen and Hao Zhang. Learning implicit fields for generative shape modeling. In *Proceedings of the IEEE/CVF Conference on Computer Vision and Pattern Recognition*, pages 5939–5948, 2019.

Minjong Lee and Dongwoo Kim. Robust evaluation of diffusion-based adversarial purification. In *Proceedings of the IEEE/CVF International Conference on Computer Vision*, pages 134–144, 2023.

Mintong Kang, Dawn Song, and Bo Li. Diffattack: Evasion attacks against diffusion-based adversarial purification. *Advances in Neural Information Processing Systems*, 36, 2024.

Francesco Croce, Sven Gowal, Thomas Brunner, Evan Shelhamer, Matthias Hein, and Taylan Cemgil. Evaluating the adversarial robustness of adaptive test-time defenses. In *International Conference on Machine Learning*, pages 4421–4435. PMLR, 2022.

Aleksander Madry, Aleksandar Makelov, Ludwig Schmidt, Dimitris Tsipras, and Adrian Vladu. Towards deep learning models resistant to adversarial attacks. *arXiv preprint arXiv:1706.06083*, 2017.

Kaiming He, Xiangyu Zhang, Shaoqing Ren, and Jian Sun. Deep residual learning for image recognition. In *Proceedings of the IEEE conference on computer vision and pattern recognition*, pages 770–778, 2016.

Alex Krizhevsky, Geoffrey Hinton, et al. Learning multiple layers of features from tiny images. 2009.

Yang Song, Jascha Sohl-Dickstein, Diederik P Kingma, Abhishek Kumar, Stefano Ermon, and Ben Poole. Score-based generative modeling through stochastic differential equations. *arXiv preprint arXiv:2011.13456*, 2020.

Jascha Sohl-Dickstein, Eric Weiss, Niru Maheswaranathan, and Surya Ganguli. Deep unsupervised learning using nonequilibrium thermodynamics. In *International conference on machine learning*, pages 2256–2265. PMLR, 2015.

Jonathan Ho, Ajay Jain, and Pieter Abbeel. Denoising diffusion probabilistic models. *Advances in neural information processing systems*, 33:6840–6851, 2020.

Yang Song and Stefano Ermon. Generative modeling by estimating gradients of the data distribution. *Advances in neural information processing systems*, 32, 2019.

F. Croce and M. Hein. Reliable evaluation of adversarial robustness with an ensemble of diverse parameter-free attacks. In *International Conference on Machine Learning*. PMLR, 2020.

Sergey Zagoruyko and Nikos Komodakis. Wide residual networks. *arXiv preprint arXiv:1605.07146*, 2017.

Karen Simonyan and Andrew Zisserman. Very deep convolutional networks for large-scale image recognition. In *International Conference on Learning Representations*, 2015.

Prafulla Dhariwal and Alexander Nichol. Diffusion models beat gans on image synthesis. *Advances in neural information processing systems*, 34:8780–8794, 2021.

Jooyoung Choi, Sungwon Kim, Yonghyun Jeong, Youngjune Gwon, and Sungroh Yoon. Ilvr: Conditioning method for denoising diffusion probabilistic models. in 2021 ieee. In *CVF international conference on computer vision (ICCV)*, pages 14347–14356, 2021.

Jin Gao, Jialing Zhang, Xihui Liu, Trevor Darrell, Evan Shelhamer, and Dequan Wang. Back to the source: Diffusion-driven adaptation to test-time corruption. In *Proceedings of the IEEE/CVF Conference on Computer Vision and Pattern Recognition*, pages 11786–11796, 2023.

Jean Feydy, Thibault Séjourné, François-Xavier Vialard, Shun-ichi Amari, Alain Trouvé, and Gabriel Peyré. Interpolating between optimal transport and mmd using sinkhorn divergences. In *The 22nd International Conference on Artificial Intelligence and Statistics*, pages 2681–2690. PMLR, 2019.

Changhao Shi, Chester Holtz, and Gal Mishne. Online adversarial purification based on self-supervision. *arXiv preprint arXiv:2101.09387*, 2021.

Jia Deng, Wei Dong, Richard Socher, Li-Jia Li, Kai Li, and Li Fei-Fei. Imagenet: A large-scale hierarchical image database. In *2009 IEEE conference on computer vision and pattern recognition*, pages 248–255. Ieee, 2009.

Nicholas Carlini and David Wagner. Towards evaluating the robustness of neural networks (2016). *arXiv preprint arXiv:1608.04644*, 2016.

Jonathan Uesato, Brendan O’donoghue, Pushmeet Kohli, and Aaron Oord. Adversarial risk and the dangers of evaluating against weak attacks. In *International conference on machine learning*, pages 5025–5034. PMLR, 2018.

Xuechen Li, Ting-Kam Leonard Wong, Ricky TQ Chen, and David Duvenaud. Scalable gradients for stochastic differential equations. In *International Conference on Artificial Intelligence and Statistics*, pages 3870–3882. PMLR, 2020.

Sylvestre-Alvise Rebuffi, Sven Gowal, Dan Andrei Calian, Florian Stimberg, Olivia Wiles, and Timothy A Mann. Data augmentation can improve robustness. *Advances in Neural Information Processing Systems*, 34:29935–29948, 2021.

Jiequan Cui, Zhuotao Tian, Zhisheng Zhong, Xiaojuan Qi, Bei Yu, and Hanwang Zhang. Decoupled kullback-leibler divergence loss. *arXiv preprint arXiv:2305.13948*, 2023.

Boya Zhang, Weijian Luo, and Zhihua Zhang. Enhancing adversarial robustness via score-based optimization. *Advances in Neural Information Processing Systems*, 36, 2024.

Ze Liu, Han Hu, Yutong Lin, Zhuliang Yao, Zhenda Xie, Yixuan Wei, Jia Ning, Yue Cao, Zheng Zhang, Li Dong, et al. Swin transformer v2: Scaling up capacity and resolution. In *Proceedings of the IEEE/CVF conference on computer vision and pattern recognition*, pages 12009–12019, 2022.

## Appendix

### A Related Works: Supplement

In Hill et al. [2020], the author proposed incorporating an energy-based model (EBM) with Markov Chain Monte Carlo (MCMC) sampling for adversarial purification. This method constitutes a memoryless sampling trajectory that removes adversarial signals, while this sampling behavior preserves image classes over long-run trajectories.

In Adaptive Denoising Purification (ADP) Yoon et al. [2021], the authors used the Noise Conditional Score Network (NCSN) with Denoising Score Matching (DSM) as the purifier, but with a deterministic short-run update rule for purification. This fixes the need for performing long-run sampling in order to remove adversarial noise in Hill et al. [2020].

Guided Diffusion Model for Purification (GDMP) Wang et al. [2022], Wu et al. [2022] is proposed to embed purification into the reverse diffusion process of a DDPM Ho et al. [2020]. GDMP submerges adversarial perturbations with gradually added Gaussian noises during the diffusion process and removes both noises through a guided denoising process. By doing so, GDMP can significantly reduce the perturbations raised by adversarial attacks and improve the robustness of classification.

### B Adversarial Attacks

Two types of adversarial attacks are briefly introduced here.

**White-box attack.** The attacker knows all information about  $f_\phi$ , including the model architecture, parameters  $\phi$ , training schedule, and so on. One of the most indicative white-box attacks is projected gradient descent (PGD) Madry et al. [2017], a gradient-based attack. It produces adversarial perturbation by projecting NN’s gradients on the clipping bound in an iterative manner. If the gradient is correctly calculated, the loss would certainly be maximized, and the NN, especially for non-robust NN, will be likely to return misclassified outputs.

**Black-box attack.** The attacker does not know all the information mentioned above in  $f_\phi$ . Common black box attack methods are roughly divided into two types: Query-base attack and Transfer-based attack.

No matter white- or black-box attack is concerned, in order to make adversarial perturbation less detectable, we will set a range of attack intensity, that is, adversarial perturbation is only allowed to perturb within a given norm value. Usually  $\ell_p$ -norm, denoted as  $\|\cdot\|_p$  ( $p = 1, 2, \infty$ ), is used:

$$\|\delta\|_p := \begin{cases} (\sum_i \delta_i^p)^{1/p} & p = 1 \text{ or } 2, \\ \max_i |\delta_i| & p = \infty. \end{cases} \quad (10)$$

In terms of intensity, we are accustomed to using  $\epsilon_p$  to represent it. For example, it often uses  $\epsilon_\infty = 8/255$  to indicate that the intensity range of currently used  $\delta$  is  $\|\delta\|_\infty \leq 8/255$ .

### C Diffusion Models: Supplement

Diffusion models were inspired by the diffusion phenomena under nonequilibrium thermodynamics in the physical world to design a framework that generates data by learning the reverse process of the data being destroyed by Gaussian noise gradually.

In the literature, the diffusion model Sohl-Dickstein et al. [2015] is a type of generative model (e.g., GAN and VAE). Conceptually, this generative process behaves like denoising. Given a data point  $x_0 \sim q$ , where  $q$  denotes the (unknown) true data distribution, and a variance schedule  $\{\beta_t\}_{t=1}^T$ , the forward diffusion process follows  $q(x_{1:T}|x_0) = \prod_{t=1}^T q(x_t|x_{t-1})$ , where  $q(x_t|x_{t-1}) = \mathcal{N}(x_t; \sqrt{1 - \beta_t}x_{t-1}, \beta_t I)$ , and the reverse diffusion process follows:

$$p_\theta(x_{0:T}) = p(x_T) \prod_{t=1}^T p_\theta(x_{t-1}|x_t), \quad (11)$$

where  $p_\theta(x_{t-1}|x_t) \sim \mathcal{N}(x_{t-1}; \mu_\theta(x_t, t), \Sigma_\theta(x_t, t))$ ,  $x_T \sim \mathcal{N}(0, I)$ , and  $\mu_\theta(x_t, t)$  and  $\Sigma_\theta(x_t, t)$  denote the mean and covariance from the diffusion model parameterized by  $\theta$  at time step  $t$ , respectively.

After that, there are several types of recently developed diffusion models, including score-based diffusion Song and Ermon [2019], Song et al. [2020], guided-diffusion Dhariwal and Nichol [2021], ILVR Choi et al. [2021], denoising diffusion probabilistic model (DDPM) Ho et al. [2020], and DDA Gao et al. [2023].

Specifically, in guided diffusion Dhariwal and Nichol [2021], given a label  $y$  as the condition and Eq. (11), the conditional reverse process is specified as:

$$p_\theta(x_0, \dots, x_{T-1} | x_T, y) = \prod_{t=1}^T p_\theta(x_{t-1} | x_t, y). \quad (12)$$

To solve Eq. (12),  $\theta$  is decomposed into two terms as  $\theta = \varphi \cup \phi$  to form separate models:

$$p_\theta(x_{t-1} | x_t, y) = Z p_\varphi(x_{t-1} | x_t) p_\phi(y | x_{t-1}), \quad (13)$$

where  $Z$  is a normalization constant. Guided-diffusion improves the model architecture by adding attention head and adaptive group normalization, that is, adding time step and class embedding to each residual block. At the same time, with reference to GAN-based conditional image synthesis, class information is added during sampling and another classifier is used to improve the diffusion generator. To be precise, the pre-trained diffusion model can be adjusted using the gradient of classifier to direct the diffusion sampling process to any label.

Score-based diffusion Song and Ermon [2019], Song et al. [2020] generates samples by estimating the gradients of unknown data distribution with score matching, followed by Langevin dynamics, moving data points to areas with higher density of data distribution. In practice, the score network  $s_\theta$  is trained to predict the true data distribution  $q$  as:

$$s_\theta(x_t, t) \approx \nabla_{x_t} \log q(x_t) = -\frac{\epsilon_\theta(x_t, t)}{\sqrt{1 - \bar{\alpha}_t}}, \quad (14)$$

where  $\bar{\alpha}_t = \prod_{s=1}^t (1 - \beta_s)$ .

On the other hand, the conditional generation of the diffusion model has also received considerable attention. In ILVR Choi et al. [2021], the author proposed a learning-free conditioning generation, which is challenging in denoising diffusion probabilistic model (DDPM) Ho et al. [2020] due to the stochasticity of the generative process. It leveraged a linear low-pass filtering operation  $\phi_N$  as a condition to guide the generative process in DDPM for generating high-quality images based on a given reference image  $c$  at time  $t$ , termed  $c_t$ , which can be obtained by the forward diffusion process  $q$ . The update rules are derived as follows:

$$\begin{aligned} x'_t &\sim p_\theta(x'_t | x_{t+1}) \\ c_t &\sim q(c_t | c) \\ x_t &\leftarrow \phi_N(c_t) - x'_t - \phi_N(\hat{x}'_t), \end{aligned} \quad (15)$$

where the factor of downsampling and upsampling is denoted as  $N$ .

DDA Gao et al. [2023] also came up with a similar approach to resolve the domain adaptation problem in the test-time scenario. The authors adapt the linear low-pass filtering operation  $\phi_N$  in ILVR Choi et al. [2021] as conditions, and their method also forces the sample  $x_t$  to move in the direction that decreases the distance between the low-pass filtered reference image  $\phi_N(x_0)$  and low-pass filtered estimated reference image  $\phi_N(\hat{x}_0)$ . The update rule is specified as follows:

$$\hat{x}_0 \leftarrow \sqrt{\frac{1}{\bar{\alpha}_t}} x_t - \sqrt{\frac{1}{\bar{\alpha}_t} - 1} \epsilon_\theta(x_t, t) \quad (16)$$

$$x_t \leftarrow \hat{x}_t - w \nabla_{x_t} \|\phi_N(x_0) - \phi_N(\hat{x}_0)\|_2, \quad (17)$$

where  $N$  is the factor of downsampling and upsampling, and  $w$  is the step size.

## D Intermediate Images Generated from Fig. 2(c)

In Fig. 5, we show the images generated from each step in Fig. 2(c) for visual inspection.

## E Algorithm in Sec. 3.3

Here, we describe the entire procedure of the proposed method in Sec. 3.3.

## F Attack Cost in Time Complexity: Detailed Analysis

In this section, we discuss the cost the attackers need to pay to defeat our proposed test-time adversarial defense method. In particular, we focus on analyzing the time complexity of defeating the diffusion-based purifiers presented in Sec. 3.2 and Sec. 3.3.

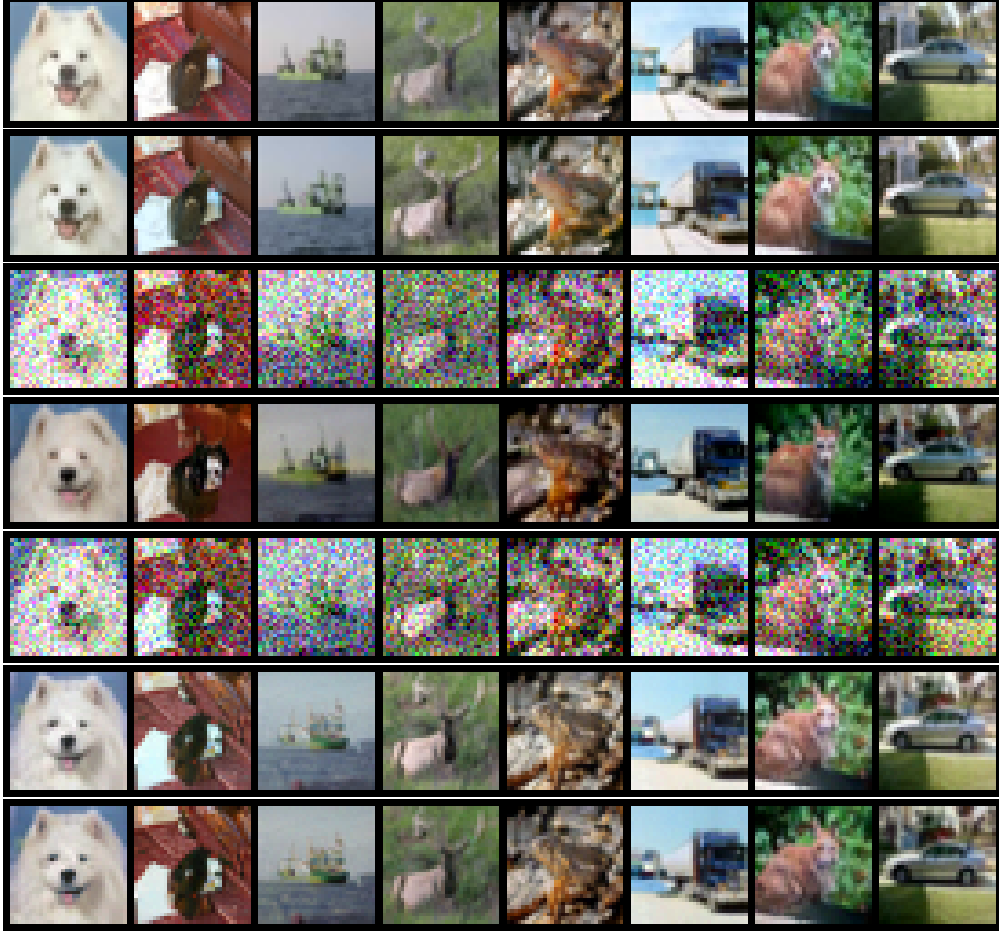


Figure 5: Intermediate Images generated from Fig. 2(c). From Top to Bottom: The images denote clean image  $x$ ,  $x^{p_2}$ ,  $x_{t^*}^{p_1}$ ,  $\widehat{x^{p_1}}$ ,  $x_{t^*}^{p_2}$ ,  $\widehat{x^{p_2}}$ , and purified image  $\widehat{x_{clean}^{p_1}}$ , respectively.

In DISCO Ho and Vasconcelos [2022], let  $N_d$  and  $N_c$  be defined as the number of parameters in DISCO and its downstream classifier, respectively. In *training time*, the authors estimated that the time complexity of defense/purification is  $\mathcal{O}(N_d)$  and that of adaptive attack (*i.e.*, designing an adversarial example by knowing the whole model) is  $\mathcal{O}(KN_d + N_c)$ , where  $K$  is the number of steps. Hence, the ratio of attack-to-defense cost in training time is  $\mathcal{O}(K + N_c/N_d)$  and the authors asserted that the time complexity of defense is much less than that of attack since  $N_d < N_c$ . In *testing time*, the time complexity of defense becomes  $\mathcal{O}(KN_d)$  (see green bars in Fig 10 of Ho and Vasconcelos [2022]) while the other remains the same. Hence, the ratio of attack-to-defense cost in testing time is  $\mathcal{O}(1 + N_c/(KN_d))$ , revealing that even  $N_c$  is larger than  $N_d$ , the time complexity for both the attacker and defender can tie if  $K$  is large enough.

In DiffPure Nie et al. [2022], the authors argued that an adaptive attack on diffusion model by traditional back-propagation would cause high memory cost. To overcome this issue, they instead applied *adjoint method* Li et al. [2020] to efficiently estimate the gradient used for designing adaptive adversarial perturbation under constant memory cost. From Table 1 in Li et al. [2020], it is asserted that, under the *tolerance*  $\epsilon = 1/T$ , the per-step time complexity scales as  $\log_2 T$ , where  $T$  is the number of steps required during the reversed process. So, the time complexity of adjoint method through the reverse diffusion process is  $\mathcal{O}(T \log_2 T)$ .

We, however, raise the concern that the presented time cost is likely to ignore one important factor: the number of parameters in a diffusion model, denoted as  $N_{dm}$ . Hence, in conservatively speaking, the time complexity of adjoint method through the reverse process should be corrected as  $\mathcal{O}(N_{dm}T \log_2 T)$ .

Based on the above concerns, our estimations of the time complexity of adversarial attack and proposed defense methods in *testing time* are described as follows. For the defense method described in Sec. 3.2, since the baseline purifier  $g_\theta$  is reused in every step of the diffusion process,  $T$  is equal to  $K$  (hereafter, we will use them interchangeably). So, the time complexity costs of adaptive attack and our defense are derived as  $\mathcal{O}(N_{dm}T \log_2 T + TN_d + N_c)$

**Algorithm 1** Diffusion Path Cleaning-based Purifier

---

**Require:** Purifier  $g_\theta$ , adversarial image  $x_{adv}$   
**Ensure:** Purified image  $\widehat{x_{clean}}$

- 1:  $x \leftarrow x_{adv}$
- 2: **for** repeated time from  $1 \dots 2$  **do**
- 3:    $x^{p_1} \leftarrow x$ ;  $x^{p_2} \leftarrow x$
- 4:    $j \leftarrow \operatorname{argmin}_{i \in \{1, \dots, C\}} S_\varepsilon(x^{p_2}, x_i^{tar})$
- 5:    $x^{p_2} \leftarrow f_{CT}(x^{p_2}, x_j^{tar})$
- 6:    $x^{p_1} \leftarrow g_\theta(x^{p_1})$ ;  $x^{p_2} \leftarrow g_\theta(x^{p_2})$
- 7:    $x \leftarrow f_{CT}(x^{p_2}, x^{p_1})$
- 8: **end for**
- 9:  $\widehat{x_{clean}} \leftarrow x$
- 10: **return**  $\widehat{x_{clean}}$

---

and  $O(N_{dm}T + N_dT + N_c)$ , respectively. In practice,  $N_{dm}$  is usually much larger than  $N_d$  and  $N_c$ , so we have  $O(N_{dm}T \log_2 T + TN_d + N_c) \approx O(N_{dm}T \log_2 T)$  and  $O(N_{dm}T + N_dT + N_c) \approx O(N_{dm}T)$ , and the ratio of attack-to-defense cost is  $O(\log_2 T)$ . Moreover, if the attacker adopts the Expectation Over Time (EOT) operation with a number of iterations,  $T_{EOT}$ , the time cost of creating such an attack has to be additionally multiplied by  $T_{EOT}$ . For example, if  $T = 100$  and  $T_{EOT} = 20$ , the ratio theoretically approximates 133; *i.e.*, the time cost of adaptive attack is around 133 times as big as that of defense.

For the defense method described in Sec. 3.3, since two diffusion paths should be maintained during purification, the time complexity is simply doubled than the one in a single path (Sec. 3.2). It is concluded that although the inference time of our proposed test-time defense methods is increased, the increased cost also complicates the adaptive attacks as well.

Table 6 shows the time cost comparison between the reverse diffusion process (purification) and adaptive attack (BPDA+20 EOT), implemented using the adjoint strategy in Sec. 3.4, under DiffPure and our defense methods. Here, we do not consider the adaptive AutoAttack since the mechanism is much more complex beyond the above analysis.

Methods	Purification Time (sec.)	Attack Time (sec.)	Ratio
DiffPure Nie et al. [2022]	35.20 $\pm$ 0.67	2508.56 $\pm$ 116.06	71.27
Sec. 3.2	34.59 $\pm$ 0.95	2504.14 $\pm$ 112.61	72.39
Sec. 3.3	72.84 $\pm$ 34.41	7517.03 $\pm$ 1970.35	103.20

Table 6: Computational time cost comparison in five runs. This evaluation utilizes four testing images with batch size two, running on one NVIDIA V100. The ratio is calculated as the average time required for BPDA+20 EOT divided by that for reverse diffusion.

## G More Experimental Results

In this section, we evaluate the robustness of our method against several  $\ell_2$ -norm and black-box attacks. Also, we examine the robustness of our method using CIFAR-100 Krizhevsky et al. [2009] and ImageNet Deng et al. [2009].

### G.1 Results on More Attacks

We tested our methods against  $\ell_2$ -norm optimization-based attacks and black-box attacks, including C&W attack Carlini and Wagner [2016], SPSA Uesato et al. [2018], and the targeted black-box attack in both settings (nonadaptive/adaptive). We utilized the Python package, called Torchattacks, to implement C&W and SPSA attacks. The results are shown in Table. 7. For the targeted black-box attack, we found that it is a special case of DiffAttack Kang et al. [2024] since it only utilizes the input image and purified image to optimize the attack direction. The results are shown in Table. 8. It can be observed that under these attacks, the robust accuracy is well maintained.

Attacks	Clean Accuracy (%)	Robust Accuracy (%)
C&W	90.62 $\pm$ 1.70	90.56 $\pm$ 1.51
SPSA	90.46 $\pm$ 1.91	90.65 $\pm$ 1.83

Table 7: Non-adaptive attacks on Sec. 3.2. Classifier: WRN-28-10. Dataset: CIFAR-10.

Attacks	Clean Accuracy (%)	Robust Accuracy (%)
Targeted attack	95.31	95.31
C&W	90.17 $\pm$ 4.31	85.09 $\pm$ 6.37
SPSA	89.32 $\pm$ 4.85	89.19 $\pm$ 4.81

Table 8: Adaptive attacks on Sec. 3.3. Classifier: WRN-28-10. Dataset: CIFAR-10.

## G.2 Results on CIFAR-100

We provide the robustness evaluation against adversarial attacks on CIFAR-100, as shown in Table 9 (*cf.* Tables 4 and 5 for CIFAR-10). Similarly, the experiments in the first block of Table 9 are under the setting of non-adaptive attack, in which the attacker only knows the information of the downstream classifier. We also excerpt the results of Rebuffi et al. [2021], Wang et al. [2023], Cui et al. [2023] from RobustBench Croce et al. [2021] for more comparisons. The second block of Table 9 shows the results obtained under the setting of adaptive attacks. Note that the results for DiffPure Nie et al. [2022] are from Zhang et al. [2024]. We can find that our methods are either better than the prior works under BPDA+EOT or comparable with DiffPure under AutoAttack and PGD- $\ell_\infty$ .

## G.3 Results on ImageNet

We provide the robustness evaluation against non-adaptive PGD- $\ell_\infty$  on ImageNet, as shown in Table 10. This experiment was conducted on a more advanced transformer-based classifier Liu et al. [2022] with  $\|\delta\|_\infty \leq 8/255$  and ResNet-50 with  $\|\delta\|_\infty \leq 4/255$ . Our method proposed in Sec. 3.3 is slightly better than DiffPure, while Our method proposed in Sec. 3.2 is comparable with DISCO, which, however, needs additional data for training EDSR for purification.

Defense Methods	Clean Acc (%)	Robust Acc (%)	Attacks
No defense	81.66	0	PGD- $\ell_\infty$
Rebuffi <i>et al.</i> Rebuffi et al. [2021]	62.41	32.06	AutoAttack (Standard)
Wang <i>et al.</i> Wang et al. [2023]	72.58	38.83	AutoAttack (Standard)
Cui <i>et al.</i> Cui et al. [2023]	<b>73.85</b>	39.18	AutoAttack (Standard)
DiffPure Nie et al. [2022]	<b>61.96±2.26</b>	59.27±2.95	PGD- $\ell_\infty$
DiffPure Nie et al. [2022]	61.98±2.47	<b>61.19±2.87</b>	AutoAttack (Standard)
Ours (Sec. 3.2)	61.71±2.49	<b>60.21±1.82</b>	PGD- $\ell_\infty$
Ours (Sec. 3.2)	62.02±2.24	60.08±2.44	AutoAttack (Standard)
<hr/>			
No defense	81.66	0	BPDA+EOT
DiffPure Nie et al. [2022], Zhang et al. [2024]	69.92	48.83	BPDA+EOT
Hill <i>et al.</i> Hill et al. [2020]*	51.66	26.10	BPDA+EOT
ADP ( $\sigma = 0.1$ ) Yoon et al. [2021]*	60.66	39.72	BPDA+EOT
Ours (Sec. 3.3)	<b>70.38±4.05</b>	<b>51.25±3.82</b>	BPDA+EOT

Table 9: Robustness evaluation and comparison between our method and state-of-the-art methods. Classifier: WRN-28-10. Testing dataset: CIFAR-100. Asterisk (\*) indicates that the results were excerpted from the papers. Boldface indicates the best performance for each attack.

Defense Methods	Clean Acc (%)	Robust Acc (%)	Classifier	Attack
DISCO Ho and Vasconcelos [2022]*	<b>72.64</b>	66.32	ResNet-50	PGD- $\ell_\infty$ (4/255)
Ours (Sec. 3.2)	69.32±12.18	<b>68.12±12.13</b>	ResNet-50	PGD- $\ell_\infty$ (4/255)
Ours (Sec. 3.3)	67.55±11.73	66.54±12.15	ResNet-50	PGD- $\ell_\infty$ (4/255)
DiffPure Nie et al. [2022]	75.13±11.67	73.11±11.76	SwinV2 Liu et al. [2022]	PGD- $\ell_\infty$ (8/255)
Ours (Sec. 3.2)	75.37±12.01	71.73±12.63	SwinV2 Liu et al. [2022]	PGD- $\ell_\infty$ (8/255)
Ours (Sec. 3.3)	<b>75.38±12.78</b>	<b>73.20±11.27</b>	SwinV2 Liu et al. [2022]	PGD- $\ell_\infty$ (8/255)

Table 10: Robustness comparison between our method and DISCO/DiffPure. Testing dataset: ImageNet. Asterisk (\*) indicates that the results were excerpted from the paper. Boldface indicates the best performance for each attack.